

Influence of Human Blocker in CDL Channel Model for 5G Millimeter Wave Communication

Jai Kumar* and Akhil Gupta

School of Electronics and Electrical Engineering, Lovely Professional University, Punjab, India
 Email: jaiky2011@gmail.com (J.K.), akhilgupta112001@gmail.com (A.G.)

Manuscript received October 29, 2024; revised December 28, 2024; accepted January 30, 2025

*Corresponding author

Abstract—The millimeter wave (mm-wave) communication has emerged as a promising technology for future wireless networks, offering the potential for high-throughput during data transmission. However, the propagation of these high-frequency signals, as well as their vulnerability to blockage, pose significant challenges in creating accurate models of the mm-wave wireless channel. One approach to modeling these wireless channels is the Cluster Delay Line (CDL) concept, which captures the channel’s multipath propagation and time-varying nature using clustering fundamentals. In our paper, we propose a CDL-based wireless channel model that customizes cluster characteristics such as Delay Spread (DS), Angle Spread (AS), and power to statistically build the channel model for a specific indoor and outdoor scenario in the mm-wave band. Consideration of human blockers causes alteration in the cluster parameters and influences the performance of the 5G communication. Quality-of-Service (QoS) parameters, such as throughput and block error rate (BLER), is used to evaluate the model’s performance for the Enhanced Mobile Broadband (eMBB) use case of 5G. We construct a link budget both with and without human blockage, assessing the impact of blockage on cell coverage based on the performance of the block error rate. Using the 5G physical layer and simulation tools, the 5G performance is analyzed in terms of throughput under the influence of blockage. The contribution of base station density and self-blocking angle has also been analyzed regarding coverage probability. The results demonstrate how blockage and cluster parameters in the CDL channel are important while designing mm-wave communication system for 5G application.

Index Terms—5G new radio, block error rate, cluster delay line, coverage probability, human blockage, link budget, mm-wave, Quality-of-Service (QoS), throughput, wireless channel model

NOMENCLATURE

Symbol	Description
2D	Two Dimensional
3D	Three Dimensional
3GPP	Third Generation Partnership Project
5G NR	Fifth Generation New Radio
AoA	Azimuth Angle of Arrival
AoD	Azimuth Angle of Departure
ABG	Alpha-Beta-Gamma
AS	Angular Spread
BS	Base Station
BLER	Block Error Rate
CRC	Cyclic Redundancy Check
CI	Close-in Path
CDL	Clustered Delay Line

DS	Dealy Spread
DKED	Double Knife-Edge Diffraction (DKED)
DOD	Degree of Departure
DOA	Degree of Arrival
DLSCH	Downlink Shared Channel
eMBB	Enhanced Mobile Broadband
FSPL	Free Space Path Loss
KED	Knife Edge Diffraction
LOS	Line Of Sight
LDPC	Low Density Parity Check
LSCP	Large Scale Parameters
MIMO	Multiple-Input-Multiple-Output
MCS	Modulation and Coding Scheme
MCD	Multipath Component Distance
MPC	Multipath Component
mm-wave	Millimeter Wave
MMSE	Minimum Mean Square Error
MKED	Multiple Knife-Edge Diffraction
NLOS	Non-Line Of Sight
OFDM	Orthogonal Frequency-Division Multiplexing
PL	Path Loss
PLE	Path Loss Exponent
PRB	Physical Resource Blocks
PPP	Poisson Point Process
PDSCH	Physical Downlink Shared Channel
QAM	Quadrature Amplitude Modulation
QoS	Quality of Service
PRB	Physical Resource Blocks
RMa	Rural Macro
RMS	Root Mean Square
SCM	Spatial Channel Model
SF	Shadow Fading
SNR	Signal to Noise Ratio
SINR	Signal-to-Interference-plus-Noise Ratio
SCCP	Small Scale Parameters
Tx	Transmitter
TDD	Time Division Duplex
TDL	Taped Delay Line
UE	User Equipment
UMa	Urban Macro
UMi	Urban Micro
URLLC	Ultra-reliable Low Latency Communication
XPR	Cross-Polarization Ratio
ZoA	Zenith angle Of Arrival
ZoD	Zenith angle Of Departure

I. INTRODUCTION

The Fifth Generation (5G) of cellular networks has seen a significant shift towards the utilization of millimeter-wave (mm-wave) frequencies, which offer the promise of high-throughput and low-latency communications under Enhanced Mobile Broadband (eMBB) and Ultra-Reliable Low Latency Communication (URLLC). However, the unique propagation

characteristics of these high-frequency bands present new challenges in channel modeling and simulation [1]. One of the most important aspects of 5G channel modeling is the temporal variability of the propagation parameters, which can have a significant impact on system performance, particularly in the context of user mobility [2]. Traditional sub-6 GHz channel models may not adequately capture the rapid signal degradation and spatial characteristics associated with mm-wave propagation. As such, there is a growing need for the development of new channel models that can accurately represent the temporal and spatial variability of the mm-wave channel, especially in the context of beamformed networks and user mobility [2].

The Cluster Delay Line (CDL) concept has been proposed as an effective approach for modeling mm-wave wireless channels, which captures the time-varying and frequency-selective nature of the channel [3]. This concept models the wireless channel as a superposition of multiple clusters, each representing a distinct propagation path. The delay, amplitude, and angular parameters of each cluster capture the key components of channel variability. This hierarchical structure allows the CDL model to capture both large-scale variations (different clusters from different reflectors) and small-scale variations (individual paths within a cluster) [4]. The large-scale parameters describe the overall channel behaviour, such as path loss, shadowing, and delay spread. The cluster-level parameters represent the channel impulse response as a superposition of distinct propagation paths or clusters, capturing the effects of multipath propagation. The ray-level parameters make the cluster-level description even more accurate by considering the different multipath components inside each cluster, such as their complex gains, angles of departure, and angles of arrival. Typically, we obtain the values of these parameters either by conducting extensive field measurements in various environments (urban, rural, and indoor) to collect real-world channel data, or by developing statistical models based on the measured data to characterize the distribution of parameters like delay spread, angular spread, and path loss.

Delay Spread (DS) describes the time dispersion of multipath components and desired value of delay spread (DS desired) mainly depends on its environment. The CDL models reflect the delay values assigned to each tap within a cluster. Angular spread describes the variation in arrival angles of multipath components within a cluster. The specific environment and scenario being modeled heavily influence the choice of distribution for both delay spread and angular spread. Researchers and engineers often use empirical data and statistical analysis to select the most appropriate distributions for their particular use case [1]. At the same time, mm-wave frequencies are also susceptible to additional parameters, including Doppler spread and blockage caused by humans. The mobility of the communication nodes induces the frequency dispersion known as Doppler spread, while the blockage characteristics of the human body (attenuation, shadowing) and their movement patterns define human blockage.

The environment has a significant impact on mm-wave propagation and, consequently, CDL parameters. Similarly, human blockers are also crucial for realistic indoor mm-wave channel modeling and simulations, especially in a dynamic environment like a classroom. Indoor environments usually have a lower delay spread than outdoor ones, but it can still be significant depending on the room size and furnishings. Indoor scenarios have moderate delay spread values, whereas outdoor scenarios are considered to have a potentially much wider delay spread, as shown in Table I, especially in urban settings [5]. On account of angular spread, indoor environments can have very complex angular spread characteristics due to reflections from walls, ceilings, and objects. Large structures and terrain strongly influence outdoor angular spread, whereas indoor cases consider wide angular spread, potentially with multiple peaks and complex distribution [6]. Indoors often incorporate specific attenuation factors for different materials, while small-scale obstacles lessen their impact in outdoor spaces. Altogether, the presence of human blockers due to static or moving people tailors the CDL model parameters to present intriguing challenges for mm-wave communication.

TABLE I: DELAY SPREAD FOR CDL MODEL

S/N*	Model	DS _{desired}
1	Very short delay spread	10 ns
2	Short delay spread	30 ns
3	Nominal delay spread	100 ns
4	Long delay spread	300 ns
5	Very long delay spread	1000 ns

* S/N: Scenario number

The major contribution of the proposed paper is given as follows:

- 1) We proposed a CDL channel model for the indoor (classroom) and outdoor (sports ground) scenarios based on the 3GPP standard.
- 2) We analyzed the proposed model using an analogous analytical model, making specific assumptions (separate from previous references) about the existence of blockage. Our current work primarily examines the pathloss and delay spread parameters of the channel model in the mm-wave band (up to 73 GHz).
- 3) We explained the clustering algorithm for multipath to estimate channel parameters realistically, and we also explain the 5G physical layer to simulate the communication chain at the link level.
- 4) We evaluated quality of service parameters in specific indoor and outdoor scenarios (limited coverage in literature) to assess the performance of 5G communication service for eMBB use cases.
- 5) Link budget estimation and deep analysis was done for block error rate (BLER)-based cell coverage, CDL throughput, and coverage probability analysis for mm-wave, with and without multiple human blockers, which was only introduced in previous literature.
- 6) We concluded that blockage impact and the importance of cluster parameters in the CDL channel are important considerations when

designing the mm-wave communication system for 5G applications.

The proposed paper is organized into five parts, with Section I providing the introduction, while Section II reviews the relevant literature. Section III presents a customized scenario-based model, system parameters, and result analysis for indoor and outdoor models is presented in Section IV under specific assumptions. Section V discusses the work's conclusion and future scope.

II. RELATED WORK

Multipath propagation, a phenomenon where the transmitted signal reaches the receiver through multiple paths with different gains and different delays, is a critical aspect of mm-wave propagation that can significantly impact the performance of these systems. The geometry-based channel model, which provides the direction of departure and arrival of the signal along with the delay, assesses signal attenuation and delay deterministic. Saleh-Valenzuela (SV) initially modeled signal copies with a similar delay range as clusters that arrive at the receiver in an indoor scenario [7]. This model takes into account a slow-time-varying channel that has a delay spread of 200 ns and an attenuation dynamic range of 60 dB. 3GPP has created a simple channel model for the current generation that accurately shows the spatial and temporal properties of 5G propagation and checks mobility key performance indicators like radio link failure, outage, and path diversity [2]. It demonstrates that the angular spread of the rays affects the beamforming gains of interfering beams, resulting in reduced SINRs.

Researchers have further explored several statistical distributions to model the delay and angular spread of the multipath components, which are crucial for understanding the channel characteristics and designing efficient communication systems. One of the most commonly used distributions for modeling delay spread in mm-wave channels is the exponential distribution. Researchers also identified that technology and project based standard channel model provides new vision in channel modeling like an increase in the number of antennas at the transmitter (Tx) and receiver (Rx), along with an optimal angular distribution of beams, improves the spectral efficiency of the MIMO system and use of mm wave band provides higher data rate [8]. On scenario-based modeling, the average delay spread is found to be below 60 nanoseconds, even in Non-Line-of-Sight (NLOS) urban settings. Additionally, the analysis of the stochastic model in the mm-wave band reports a normalized average angular spread of under 400 in the azimuth arrival direction [9].

Short wavelengths are vulnerable to blockage and are the primary cause that degrades the performance of mm-wave systems in varied propagation environments. We intend to consider the human body as the main contributor to reducing the efficiency of mm-wave communication [10]. The dielectric properties of the human body are crucial in studying the peculiarities of mm-wave propagation. Therefore, the human body's

obstruction generates a significant signal loss in mm-wave transmissions. The human blockage models include the cylindrical model, the Double Knife-Edge Diffraction (DKED) model, the wedged plate model, and the Multiple Knife-Edge Diffraction (MKED) model. [11] provides a comprehensive summary of these models, examining how the static and moving (0.5 m/s to 2 m/s) states of the human blocker impact the signal attenuation value and network coverage. These models carry out 2D and 3D modeling of the human body, enabling the adjustment of various channel parameters. The minimum BS deployment can improve the coverage probability by reducing the density of human blockers [12]. In [13], researchers introduced a unique approach to capture the impact of blockage probability and demonstrate the optimal transmitter height.

Momo and Mowla [14] looked at how human blocking the channel affects its statistics, like the root mean square (RMS) delay spread and pathloss, at frequencies of 28, 38, 60, and 73 GHz. Human attenuation's impact on 5G physical layer communication performance is also assessed by 3GPP channel model link simulation [15] where various blockage regions are examined to see how human blockage affects the CDL channel model and 5G millimeter wave communication.

High mobility 5G NR physical layer system for non-terrestrial network [16] applied various 5G NR numerology, modulation method, and MIMO configuration in link level simulation. The use of 3GPP Taped Delay Line (TDL) channel model with practical channel estimation, accessed the Bit error rate, throughput and spectral efficiency. Analyzed impact of human body blocker in mm-wave at 60 GHz in the meeting room, limited coverage to propagation loss, human blockage losses 24-26 dB, used beamforming to get a reflecting path as a solution to blockage [17].

Multiple sessions of measurement were conducted in [18] to examine the temporal fluctuations caused by the shadowing of human motion. Human body shadowing has a significant impact on received power and path loss. The human body's high penetration has a significant impact on path loss, channel throughput, and sum-rate. In the millimeter range, each human body may introduce a signal attenuation of around 20 dB to the transmitted power [10]. The 3GPP model looked at the blocking angle (angle of position) of people who are blocking in both self-blockage and non-self-blockage situations to figure out how the signal weakens in the 5G enhanced mobile broadband eMBB use case [19]. Similarly, another study [20] argues that the existence of human obstacles between the user and the BS causes a significant decrease in the data transfer rate at the 5G NR air interface, and it is more dominant on operating at 28 GHz [21].

The CDL model has emerged as a promising approach to address this challenge, as it allows for a more detailed representation of the spatial and temporal characteristics of the channel. Using appropriate statistical distributions, we can model the signal's angular and delay spread within the cluster delay line framework. Recent research has looked into how other distributions, like the η - μ and

κ - μ fading models [19], to describe the angular and delay spread in 5G channels. In [19], 3GPP proposed cluster delay line CDL-based channel models to improve the coverage of 5G multipath channel modeling. Some of the parameters that make up the CDL-based model are delay spread, angular spread, cluster delays, cluster powers, the Rice factor (in Line of Sight (LOS)), the angles at which each cluster leaves and arrives, and the Cross-Polarization Power Ratio (XPR). These are all generated randomly from statistical distributions for channel analysis under five different profiles. The term XPR, which measures the ratio between the pathloss without any polarization change and the pathloss when the wave receives orthogonal polarization [15], contributes

significantly to describing the channel's 3D characteristics. The CDL-based channel model is also capable of analyzing blockage phenomena via blockage models A and B.

Modeling channel characteristics is important in the evaluation of 5G new radio (5G NR) systems. This implies the need to update traditional fading distributions such as Rayleigh, Rician, Nakagami, and others to incorporate the significant high-frequency phenomenon of diffuse scattering [22]. A Summary (year wise) of important existing literature in channel modeling is given in Table II.

TABLE II: SUMMARY OF EXISTING LITERATURE

Ref. No.	Paper title and author	Year	Paper Content
[3]	Propagation Models and Performance Evaluation for 5G Millimeter-Wave Bands. By Shu Sun, Theodore S. Rappaport, <i>et al.</i> IEEE	2018	Covered channel models of 5G design, path loss model, large-scale and small-scale fading model, and MIMO channel model. Analyzed mm-wave, NYUSIM and 3GPP channel models for diverse applications under parametric values at 28 GHz. Shown max coverage distance of BS as a function of BS antenna element. Identified channel performance metrics are extremely sensitive to choice of channel models.
[14]	Effect of Human Blockage on an Outdoor mmWave Channel for 5G Communication Networks. By Sumaiya Momo, M M Mowla <i>et al.</i> , IEEE	2019	Introduced outdoor channel model, mm-wave utilization, new input parameters using human blockers; simulated knife edge diffraction model for human blockers. Identified blocker density affects received power, path loss, and RMS delay spread. At 38 GHz received power varying from -145 dBm to -85 dBm on human blockage.
[2]	Low Complexity Channel Model for Mobility Investigations in 5G Networks. By U Karabulut, A Awada <i>et al.</i> IEEE	2020	Presented channel model to adopt mobility of the user and consider spatial and temporal characteristics, low complex model found better results from Jake's model, identified Multipath beam-forming gain result in interference.
[15]	Impact of Human Blockage on 5G Communication System in the 26 GHz Band. By H Dembele, Marie Le Bot <i>et al.</i> , IEEE	2021	Evaluated impact of human blockage on 5G at 26 GHz by 3GPP, performance in BLER with and without the influence of human blockage; evaluated the impact of blockage on the cell coverage. Identified blockers reduce the cell coverage and contribute to signal attenuation.
[11]	A Survey on the Effects of Human Blockage on the Performance of mm- Wave Communication Systems. By A Alyosef, S Rizou <i>et al.</i> , IEEE	2022	Analyzed effect of human blockage in mm-wave via various human blockage models like KED, MKED, wedge plate model. Considered effect on network coverage and received power by blockage for Quality of service and also identified the potential solution to reduce the effect of blockage.
[16]	5G-NR Physical Layer-Based Solutions to Support High Mobility in 6G Non-Terrestrial Networks. By Chaitali J. Pawase <i>et al.</i> Drones 7, MDPI	2023	Analyzed high mobility system of 5G NR physical layer for a non-terrestrial network via 5G NR numerology, modulation scheme, and MIMO application analyzed. Simulated link level using practical channel estimation in the 3GPP taped delay line (TDL) model, BER, throughput, and estimated spectral efficiency.
[17]	Wideband Measurement and Analysis of Human blocking on Indoor channel at 60 GHz. By M Dieng, G Zaharia <i>et al.</i> , IEEE	2024	Analyzed impact of human body blocker in mm-wave at 60 GHz in the meeting room, limited coverage to propagation loss, human blockage losses 24-26 dB, used beamforming to get a reflecting path as a solution to blockage.
	Proposed paper	2024	Analyzed CDL channel model with human blockage for 5G application in 3GPP standard, customized channel parameters for indoor and outdoor scenarios, analyzed multiple human blockers via blockage model A, the impact of DS in throughput of 5G NR. Covered analysis in blockage.

III. CUSTOMIZED CLUSTER DELAY LINE-BASED CHANNEL MODEL

Traditional, generalized channel models often require a more accurate representation of the specific characteristics of certain propagation environments. This is where customized CDL models come in to capture unique channel characteristics, improve simulation accuracy, and adhere to emerging technologies. We can tailor this customization to accurately reflect specific features such as path loss, delay spread, and angle of arrival for various environments such as indoor factories and dense urban areas. Customized CDL models also lead to more reliable simulation results, which are essential for

evaluating system performance and optimizing system design. In essence, customized CDL models bridge the gap between theoretical models and real-world complexity, enabling more accurate simulations and better-performing communication systems.

This part of the article covers the basic characteristics of the CDL channel model for specific indoor and outdoor scenarios that consider a particular value of these characteristics. It also discusses how to estimate channel and cluster parameters, the extraction method for multipath components, the clustering algorithm, and how to make the CDL channel model fit your needs using 3GPP TR 38.901. In mm-wave channels, the scattering effects become more prominent, and the spatial

representation of the received signal clusters becomes an important consideration. The cluster delay line model is a promising way to reduce the problem of delay and angular spread in the cluster. It sees the wireless channel as a mix of several propagation paths, each with its own delay and angular characteristics [23].

A. Indoor and Outdoor Channel Model

Indoor areas are generally characterized by low effective base station (BS) height and typical deployment scenarios, covering office environments, corridors, classrooms, and shopping malls. Indoor places may have wave guide propagation effects under LOS circumstances, caused by numerous reflections off walls, roofs, ceilings, and grounds. In these scenarios, we mount the BS on a wall or ceiling at a height of 2 to 3 meters, while the height of the user equipment is 1.5 meters, and the approximate dimensions of the indoor space are 120m×50m×3m. The literature on indoor 5G wireless networks refers to the close-in path (CI) model, the 3GPP model, and the alpha-beta-gamma (ABG) model as large-scale propagation measurements for path loss estimation in indoor areas [24, 25]. Table III shows some specifications for these indoor channel models.

TABLE III: SPECIFICATIONS OF INDOOR CHANNEL MODEL

Channel model	Max distance	Frequency range	Support of mm-wave
3GPP TR38.901 [19]	1 m to 150 m	0.5 GHz to 100 GHz	Yes
ABG Model [23]	3.9 m to 45.9 m	Up to 73.5 GHz	Yes
Close-in model [24]	3.9 m to 45.9 m	Up to 73.5 GHz	Yes

In environments such as shopping malls and workplaces, several measurements from the CI model show that the route loss exponents for a one-meter free space reference distance are never more than two. This indicates that the CI path loss (PL^{CI}) is better than what is predicted by Friis' loss formula for free space, as given in (1):

$$PL^{CI}(f, d)[dB] = FSPL(f)[dB] + 10n \log_{10}(d) + \chi_{\sigma}^{CI} \quad (1)$$

where $FSPL(f, 1\text{ m}) = 20 \log_{10}(4\pi\lambda)$ is the free space path loss at 1m distance, λ is wavelength of carrier frequency, d is Tx-Rx separation distance $d \geq 1\text{ m}$, n is path loss exponent (PLE), χ_{σ}^{CI} denotes a Gaussian random variable with a zero mean and a standard deviation of σ . Similarly, for ABG model PL (PL^{ABG}) can be calculated by (2):

$$PL^{ABG}(f, d)[dB] = 10\alpha \log_{10}\left(\frac{d}{1\text{m}}\right) + \beta + 10\gamma \log_{10}\left(\frac{f}{1\text{GHz}}\right) + \chi_{\sigma}^{ABG} \quad (2)$$

where Tx-Rx separation distance $d \geq 1\text{ m}$ and operating frequency $f \geq 1\text{ GHz}$, α , β and γ are coefficients showing the dependence of path loss on distance and frequency, respectively, and β is an optimized offset (floating) value for path loss in dB. For large indoor distances (greater than 50 m) in an indoor hotspot/office (InH-office) or shopping mall, dual-slop ABG mode can be used for 5G

performance evaluation [26]. Another model, the 3GPP indoor model, provides path loss for LOS and NLOS conditions, as given in (3) and (4):

$$PL_{\text{InH-LOS}} = 32.4 + 17.3 \log_{10}(d_{3D}) + 20 \log_{10}(f_c) \quad (3)$$

$$PL_{\text{InH-NLOS}} = 17.3 + 38.3 \log_{10}(d_{3D}) + 24.9 \log_{10}(f_c) \quad (4)$$

where $1\text{ m} \leq d_{3D} \leq 150\text{ m}$ for (3) and (4), f_c is carrier frequency, distance $d_{3D} = \sqrt{d_{2D}^2 + (h_{BS} - h_{UE})^2}$ is illustrated in Fig. 1, NLOS case takes a shadow parameter σ_{SF} value of 8.03 [19].

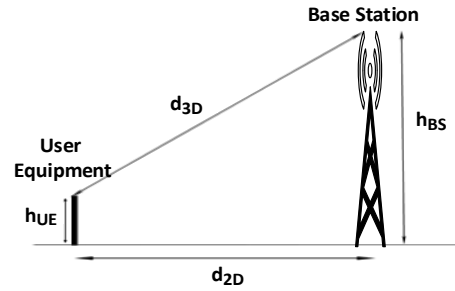


Fig. 1. Representation of d_{3D} , d_{2D} , h_{BS} and h_{UE} .

These large-scale parameters are also evaluated by the CDL channel model, and work [5] shown the effect of delay spread on the 5G performance for an indoor scenario using CDL and TDL, through link level simulation. The spatial channel model, including Winner-II, 3GPP, and METIS, also analyses the small-scale parameters like cluster delay, cluster power, polarization, doppler shift, coherence bandwidth, and angular parameters of the indoor channel model. In [15], we studied the variation in cluster power via CDL channel analysis, and evaluate 5G performance for this variation in cluster power using the blockage effect. Previous papers have also shown that polarization discrimination in indoor mm-wave channels ranges from 15 dB to 25 dB [27]. Additionally, studies have observed a more pronounced polarization discrimination of 27 dB, at 73 GHz compared to 28 GHz [28] and measured max delay spread 19 ns (28 GHz) and 288 ns (73 GHz) [29]. Observations reveal several similarities across a wide spectrum of frequencies concerning angular spread and delay spread, which are attributes of small-scale parameters. We analyzed the performance of an indoor mm-wave network in a meeting room under the influence of a human blocker, observing attenuation due to the human body's blocking losses at 60 GHz, which ranged from 24 to 26 dB [17].

An outdoor scenario is characterized by a medium-to-large open area with BS placed above the rooftop, on a lamp post, or on a 25-meter tower above the ground. These deployment scenarios cover a street canyon, an open playground, a cross street, and a backhaul in an urban area. Outdoor scenarios present unique challenges for 5G communication due to the complex nature of signal propagation, which is characterized by weather conditions, terrain, buildings, path loss, shadowing, and multipath. For outdoor 5G communication in the mm-wave range, atmospheric absorption, foliage penetration

loss, obstructions, antenna deployment through MIMO, and interference techniques for a very dense network are all things that need to be thought about. Our study takes into account an open-roof sports ground with a radius of 250 m, an inter-sight (BS-BS) distance of 500 m, a base station situated on a tower with a height of 25 m, and a minimum BS-UE distance of 35 m with a UE height of 1.5 m. Literature on outdoor 5G wireless networks covered the 3GPP TR38.901 (UMi (urban microcellular), UMa (urban macrocellular), and RMa (rural macrocellular)) [19], WINNER-II models [30], and METIS model (measurement-based) [31, 32]. Table IV shows some specifications for these outdoor channel model.

TABLE IV: SPECIFICATIONS OF OUTDOOR CHANNEL MODEL

Channel model	Max distance	Frequency Range	Support of mm-wave
3GPP TR38.901 [19]	10 km	0.5 GHz to 100 GHz	Yes
WINNER-II [30]	10 km	2 GHz to 6 GHz	No
METIS [31, 32]	1 km	10 GHz to 86 GHz	Yes

Extensive propagation measurements for the outdoor urban micro-cellular (UMi) street canyon scenario at mm-wave frequencies of 28 GHz and 73 GHz [24] show that path loss in outdoor environments with PLE 3.4 is less dependent on frequency. Analysis of the UMi and UMa scenarios, using ray tracing for large-scale parameters discovered that the environmental factor influenced the performance of these scenarios. In UMa scenario it was observed that a decrease in the delay and azimuth angle spreads an increase in frequency [33], and carrier frequency also affects a small-scale parameter, the cross-polarization discrimination ratio (XPR), which varied from 13.87 to 7.89 dB when moving from 5.6 GHz to 73.5 GHz. Outdoor RMa scenario performance is better in dual polarization than single polarization in various antenna configurations using the CDL model, and rural environments show less delay spread with higher spatial correlation [34]. Link-level simulations for the outdoor channel models UMi, UMa, and RMa [5] looked at how delay spread affected 5G performance, similar to the indoor model, and found that outdoor channels offer a broader delay spread range in RMa scenarios and significantly enhance performance by optimizing the delay. Researchers used mm-wave to study what happened when people blocked the waves outside. The RMS DS changed a lot between 0 ns and 0.9 ns at 73 GHz and between 0 ns and 0.6 ns at 38 GHz when people were present between the Tx-Rx link [35].

Pathloss for UMa scenario of LOS environment in 3GPP under parameters of shadow fading value 4, UE height range $1.5 \text{ m} \leq h_{\text{UE}} \leq 22.5 \text{ m}$ and $h_{\text{BS}} = 25 \text{ m}$ is given in (5):

$$PL_{\text{UMa-LOS}} = \begin{cases} PL_1 & 10 \text{ m} \leq d_{2D} \leq d'_{\text{DB}} \\ PL_2 & d'_{\text{DB}} \leq d_{2D} \leq 5 \text{ km} \end{cases} \quad (5)$$

and

$$PL_1 = 28.0 + 22 \log_{10}(d_{3D}) + 20 \log_{10}(f_c) \quad (6)$$

$$PL_2 = 28.0 + 40 \log_{10}(d_{3D}) + 20 \log_{10}(f_c)$$

$$9 \log_{10} \left((d'_{\text{DB}})^2 + (h_{\text{BS}} - h_{\text{UE}})^2 \right) \quad (7)$$

where $d'_{\text{DB}} = 4h_{\text{BS}}h_{\text{UE}}(\frac{f_c}{c})$ is breakpoint distance, h_{BS} and h_{UE} are the effective height of BS and UE respectively.

B. Clustering in Multipath

Clustering in multipath environments generally serves to improve the performance and efficiency of data transmission by load balancing, fault tolerance and reliability, energy efficiency, scalability, and reducing latency. The specific purpose and benefits of clustering in multipath environments can vary depending on the network architecture, application requirements, and the clustering algorithms employed.

Primarily the concept of a cluster and the framework of a cluster delay line were considered in [36], focusing on a single cluster functioning as an interface between the BS and User Equipment (UE) in a wireless channel. Furthermore, the complete analysis of the cluster-based model continues, focusing on groups of similar characteristics within the cluster and also taking into account inter-cluster characteristics. Angle spread, delay spread, and cluster gain are crucial parameters to determine the complexity and performance of wireless signal transmission. Before we can guess how well the system works, we need to get the Small-Scale Channel Parameters (SSCPs) of the multipath components using the Space-Alternative Generalized Expectation maximization (SAGE) algorithm [37]. During statistical estimation, the SAGE algorithm estimates MPC parameters sequentially, alternating between numerous tiny hidden data spaces established by the algorithm creator. In [38], they presented an improvement to the SAGE algorithm by modifying the antenna gain pattern using a more detailed model. The large-scale channel parameters (LSCP) may be calculated from statistical analysis of $s(\rho_{l,k})$. In the k th observation position, the single-wave received signal is given by (8).

$$s(\rho_{l,k}) = c(\phi_{l,k})a_{l,k} \exp(j2\pi v_{l,k}) u(t - \tau_{l,k}) \quad (8)$$

where $\phi_{l,k}, a_{l,k}, v_{l,k}, \tau_{l,k}$ are SCCPs (set of the l th path) parameters, ϕ is the azimuth angle of arrival (AoA), v is the Doppler frequency, a is the amplitude, $u(t)$ is the reference signal, $c(\phi)$ is the steering vector, τ is the delay [39].

For the time delay spread, the average access delay ($\bar{\tau}_k$) is first order statistical result and the root mean square DS is calculated as (9)

$$\text{RDS} = \sqrt{\frac{\sum_{l=1}^{l_k} \rho_{l,k} \tau_{l,k}^2}{\sum_{l=1}^{l_k} \rho_{l,k}} - \bar{\tau}_k^2} \quad (9)$$

Similarly, the root mean square of angular spread (RAS) can be calculated as given as (10), where $\psi_{l,k}(\Delta)$ is angular limit in azimuth coordinate.

$$\text{RAS} = \sqrt{\frac{\sum_{l=1}^{l_k} (\psi_{l,k}(\Delta))^2 \rho_{l,k}}{\sum_{l=1}^{l_k} \rho_{l,k}}} \quad (10)$$

The SAGE algorithm extracts MPC, which is then grouped into clusters using the K-power means algorithm. This algorithm treats the distance between MPCs as a parameter and identifies each cluster in the MPC's delay-angular domain. Since cluster-based channel models use two distinct sets of parameters: inter-cluster parameters, which describe different clusters, and intra-cluster parameters, which describe the rays inside each cluster, The inter-cluster parameter guesses the peak power of each cluster to find the strongest MPC in each one. The clusters are modeled using a truncated normal distribution and a cluster decay constant. The multipath component distance (MCD)-based process takes into account for cluster groups [39] and MCD calculations between i th and j th. MPC is done as

$$MCD_{i,j} = \sqrt{MCD_{AoA,i,j}^2 + MCD_{\tau,i,j}^2} \quad (11)$$

Corresponding AoA and τ in MCD denote in angular and delay domain MCD. This process involves three steps as listed below.

- 1) Select a point of reference for the MPC with the highest power among all the MPCs in the eligible set.
- 2) Establish a predetermined threshold labeled MCD-th and a delay scaling factor designated as ξ . Proceed to compute the MCDs between the reference MPC and the remaining elements within the collection set. Choose the MPCs with MCDs that are lower than the specified MCD threshold. Then, combine these MPCs with the reference MPC to form a single cluster.
- 3) Once you have assigned all the MPCs to specific clusters, deallocate the assigned MPCs from the MPC set and repeat Step 1 to find the next cluster.

Here, we validated the number of clusters using the Kim-Parks index. The Kim-Parks index, or KP, is a normalized version of the Davies-Bouldin index [38]. The calculation involves the use of an over-partition and under-partition measure function, v_0 and v_u which are normalized based on the lowest and maximum number of clusters C_{\min} and C_{\max} .

$$KP(C) = v_0(C) + v_u(C) \quad (12)$$

and for a particular scenario, the optimal number of clusters is given by (13)

$$C_{\text{opt}} = \underset{C}{\operatorname{argmin}}\{KP(C)\} \quad C_{\min} \leq C \leq C_{\max} \quad (13)$$

In practice, we choose the maximum number of clusters to be sufficiently large to accurately identify the proper number of clusters. Simultaneously, ray-tracing results or a stochastic approach can estimate the delay and angular spread. The stochastic model represents the cluster angles using conditional probabilities. We represent the cluster delays (τ_k) using a model based on the exponentially distributed inter-arrival times of

clusters and calculating the cluster elevation angles (θ_k) using a joint probability density function (pdf) that takes into account the elevation angles conditioned on the cluster delay. The joint PDF is represented as

$$F(\tau_k, \theta_k) = f(\theta_k|\tau_k)f(\tau_k) \quad (14)$$

where $f(\tau_k|\theta_k)$ represents the conditional pdf for the cluster elevation and $f(\tau_k)$ represents the marginal pdf for the cluster delay. The conditional probability density function (pdf) is obtained by empirical analysis, taking into account the potential elevation angles for first and second-order reflections in a room of certain dimensions. The intra-cluster angles were computed by subtracting the ray angles from the corresponding cluster centroid angles. The estimated variances σ for the azimuth intra-cluster angles for the degree of departure (DoD) and degree of arrival (DoA) were 0.7 and 0.3 radians, respectively. Similarly, the values of σ for DoD and DoA were calculated to be 0.2 and 0.3 radians, respectively, for the elevation intra-cluster angles. A novel spectral clustering algorithm also presented in [40] provides improved performance in complex structured clusters in densely noisy environments.

C. Cluster Delay Line Channel Model

The CDL channel model is a statistical approach that accurately characterizes the wireless channel's time-varying and frequency-selective nature, particularly in environments with clustered multipath components. CDL models account for the temporal dispersion effects resulting from multipath propagation by segmenting the delayed signal path into clusters. Each cluster denotes a collection of similarly situated signal paths with comparable propagation characteristics [41]. The CDL model often implies spatial consistency over a certain distance, indicating that the channel properties stay relatively constant throughout a small region. Nevertheless, the characteristics may undergo alterations while transitioning to a distinct geographical area. The CDL model incorporates the time-varying characteristics of the wireless channel, recognizing that the propagation conditions might alter over time as a result of movement or environmental factors.

Our proposed work mainly considers a standardized channel model named the 3rd generation partnership project (3GPP), which has published a technical study on channel models for frequencies ranging from 0.5 to 100 GHz that are intended for use in future 5G and beyond channel modeling. The technical study aims to aid in the modeling and assessment of physical layer approaches by using appropriate channel models in succession to previous approaches. The CDL channel models proposed in this study for link-level simulations for the evaluation of 5G systems in the full frequency range from 0.5 to 100 GHz [19]. Fig. 2 uses the cluster technique to show the multipath propagation between the transmitter (Tx) and receiver (Rx).

The CDL channel models are an expansion of the Taped Delay Line (TDL) profiles, specifically created for

three-dimensional channels with a quasi-deterministic method. There are five distinct CDL profiles covering LOS and NLOS scenarios, regarding non-line-of-sight (NLOS) scenarios, there exist three distinct models known as CDL-A, CDL-B, and CDL-C. whereas LOS scenarios consider CDL-D and CDL-E profiles. These predefined CDL profile are tabled for providing various CDL parameters along-with extendable consideration of blockage in the channel model. Parameters denote the elevation (or zenith) angle of departure, the elevation angle of arrival, the azimuth angle of departure, and the azimuth angle of arrival, respectively, for the m th ray of the n th cluster in the global coordinate system, with the BS as the transmitter and the UE as the receiver. A total of 20 rays composes each cluster, and some of the cluster parameters are listed in Table V.

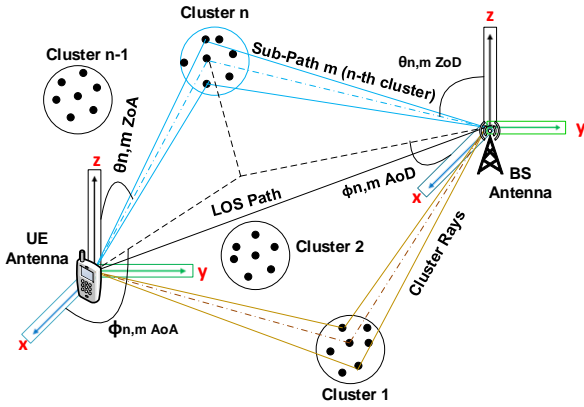


Fig. 2. Clusters in multipath propagation.

TABLE V: CLUSTER DELAY LINE PARAMETERS

S/N	Parameter	Value/ Description
1.	Number of clusters	24 (NLOS) and 14 (LOS)
2.	Number of Rays per cluster	20
3.	$\bar{\tau}_k$	Delay Spread
4.	$\phi_{n,AoD}$	Azimuth angle of departure
5.	$\phi_{n,AoA}$	Azimuth angle of arrival
6.	XPR	Cross-polarization power ratio
7.	$H(t,r)$	Channel coefficient
8.	Antenna configuration	MIMO

While generating channel coefficients for the CDL profiles, the first step involves generating the azimuth angles of departure and arrival. Therefore, we can obtain the arrival angles for the m th ray of the n th cluster by

$$\phi_{n,m,AoA} = \phi_{n,AoA} + C_{ASA}\alpha_m \quad (15)$$

where $\phi_{n,AoA}$ denotes the azimuth angle of arrival (AoA), C_{ASA} is the azimuth spread of the arrival angle and α_m is the ray offset angle within a cluster. A similar equation is also used to generate the angles of departure as given in (16):

$$\phi_{n,m,AoD} = \phi_{n,AoD} + C_{ASD}\alpha_m \quad (16)$$

where $\phi_{n,AoD}$ denote the azimuth angle of departure (AoD) and C_{ASD} denotes the cluster-wise root mean square (RMS) azimuth spread of departure angle. Further,

the generation of the $\theta_{n,m,ZoA}$ zenith angle of arrival (ZoA) and $\theta_{n,m,ZoD}$ zenith angle of departure (ZoD) angles is analogous to the Eqs. (15) and (16), respectively. The $\phi_{n,m,AoD}$ AoD angles are randomly coupled with the $\phi_{n,m,AoA}$ AoA angles within a cluster. The $\theta_{n,m,ZoD}$ ZoD angles are also randomly coupled with the $\theta_{n,m,ZoA}$ ZoA angles. The cross-polarization power ratio (XPR), k , is derived for each m th ray of each n th cluster:

$$k = 10^{\frac{\zeta}{10}} \quad (17)$$

where ζ is the cross polarization for each cluster in dB. Lastly, the channel coefficients for each n th cluster and Tx-Rx antenna element pair (t, r) for a NLOS environment are given by (18).

$$H_{r,t,n}^{NLOS}(t) = \sqrt{\frac{P_n}{M}} \sum_{m=1}^M \begin{bmatrix} F_{R_{x,r},\theta}(\theta_{n,m,ZoA}, \phi_{n,m,AoA}) \\ F_{R_{x,r},\phi}(\theta_{n,m,ZoA}, \phi_{n,m,AoA}) \end{bmatrix}^T \times \begin{bmatrix} e^{j\phi_{n,m}^{\theta\theta}} & \sqrt{k_{n,m}^{-1}} e^{j\phi_{n,m}^{\theta\phi}} \\ \sqrt{k_{n,m}^{-1}} e^{j\phi_{n,m}^{\phi\theta}} & e^{j\phi_{n,m}^{\phi\phi}} \end{bmatrix} \begin{bmatrix} F_{T_{x,t},\theta}(\theta_{n,m,ZoD}, \phi_{n,m,AoD}) \\ F_{T_{x,t},\phi}(\theta_{n,m,ZoD}, \phi_{n,m,AoD}) \end{bmatrix} \times e^{\frac{j2\pi(\hat{n}_{R_{x,n,m}}^T \hat{d}_{R_{x,r}})}{\lambda_0}} e^{\frac{j2\pi(\hat{n}_{T_{x,n,m}}^T \hat{d}_{T_{x,t}})}{\lambda_0}} e^{\frac{j2\pi(\hat{n}_{R_{x,n,m}}^T \hat{v}_t)}{\lambda_0}} \quad (18)$$

where $F_{R_{x,r},\theta}$ and $F_{R_{x,r},\phi}$ denote the field radiation patterns of the receiver antenna element r , and $F_{T_{x,t},\theta}$ and $F_{T_{x,t},\phi}$ are the field radiation patterns of the transmitter antenna element t [42]. Here within the n th cluster, there are M number of rays, where M equals 20 in the NLOS case, $\hat{d}_{R_{x,r}}$ and $\hat{d}_{T_{x,t}}$ define the location vector of the receiver and transmitter antenna elements r and t , correspondingly. The wavelength of the carrier frequency is denoted as λ_0 and $\hat{n}_{R_{x,n,m}}^T$ indicates the spherical unit vector with the azimuth arrival angle and zenith arrival angle, $\phi_{n,m,AoA}$ and $\theta_{n,m,ZoA}$ respectively, as given in (19).

$$\hat{n}_{R_{x,n,m}} = \begin{bmatrix} \sin \theta_{n,m,ZoA} \cos \phi_{n,m,AoA} \\ \sin \theta_{n,m,ZoA} \sin \phi_{n,m,AoA} \\ \cos \theta_{n,m,ZoA} \end{bmatrix} \quad (19)$$

Similarly, the spherical unit vector, $\hat{n}_{T_{x,n,m}}$, with the azimuth and zenith departure angle, $\phi_{n,m,AoD}$ and $\theta_{n,m,ZoD}$, respectively as in (20).

$$\hat{n}_{T_{x,n,m}} = \begin{bmatrix} \sin \theta_{n,m,ZoD} \cos \phi_{n,m,AoD} \\ \sin \theta_{n,m,ZoD} \sin \phi_{n,m,AoD} \\ \cos \theta_{n,m,ZoD} \end{bmatrix} \quad (20)$$

The channel response of NLOS environment is given as per (21) as shown below.

$$H_{u,s}^{NLOS}(t, \tau) = \sum_{n=1}^N H_{u,s,n}^{NLOS}(t) \delta(\tau - \tau_n) \quad (21)$$

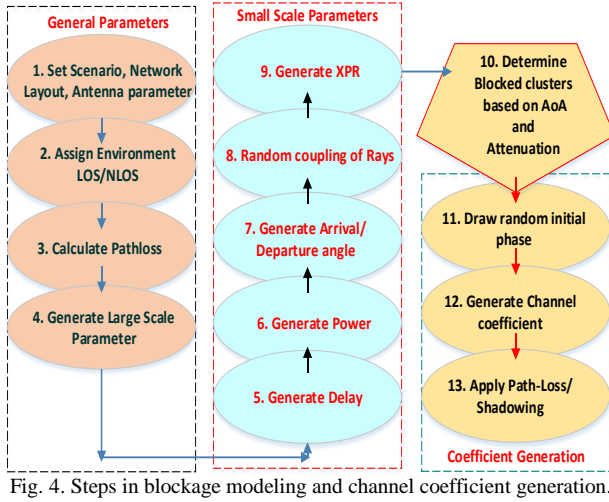


Fig. 4. Steps in blockage modeling and channel coefficient generation.

Applying the blockage model includes additional steps in channel generation, as illustrated in Fig. 4, and adapts specific and more realistic blocking Model B for further analysis. After selecting the scenario, we assigned an environment and then estimated the path loss using large-scale parameter generation. Next, we generate small-scale parameters such as cross-polarization, ray coupling, power, delay, and angle. Blockage modeling primarily involves an additional Step 10, as illustrated in Fig. 4, in the generation of channel coefficients, which takes into account the blocked cluster parameters for their AoA and attenuation. We follow Step 11 to Step 13 of Fig. 4 as a standard procedure for generating channel coefficients without any blockage.

1) 3GPP blockage model B

Standard blockage model B by 3GPP utilizes a geometric approach to accurately detect and capture instances of human or vehicular obstruction [15]. It follows the steps as described below.

Determines blockers: The map is physically occupied by a certain number, K of rectangular screens that serve as blockers. Each screen has dimensions defined by its height (h_k) and width (w_k), with the screen center located at a certain point (x_k, y_k, z_k). Suggested parameters for typical blockers are given in Table VI and are used as per the need for a specific study. Here only K -nearest blockers are considered, as the blocking effect diminishes with increasing distance to the blocker.

TABLE VI: BLOCKER PARAMETERS FOR BLOCKAGE MODEL B

Scenario	Typical set of blockers	Blocker dimensions	Mobility pattern
Indoor, Outdoor	Human	Cartesian: $w = 0.3$ m; $h = 1.7$ m	Stationary or up to 3 km/h
Outdoor	Vehicle	Cartesian: $w = 4.8$ m; $h = 1.4$ m	Stationary or up to 100 km/h

Determine the blockage attenuation per sub-path: We model the attenuation resulting from each blocker on each sub-path using a basic knife edge diffraction (KED) model. This diffraction model provides shadowing caused by each side (h_1, h_2, w_1, w_2) for the NLOS scenario, and it is calculated as per (27) and (28).

$$F_{h_1|h_2} = \frac{\arctan\left(\pm \frac{\pi}{2} \sqrt{\frac{\pi}{\lambda} (D_{2h_1|h_2} + D_{1h_1|h_2} - r)}\right)}{\pi} \quad (27)$$

$$F_{w_1|w_2} = \frac{\arctan\left(\pm \frac{\pi}{2} \sqrt{\frac{\pi}{\lambda} (D_{2w_1|w_2} + D_{1w_1|w_2} - r)}\right)}{\pi} \quad (28)$$

where $F_{h_1|h_2} = F_{h_1}$ or F_{h_2} and similar are the knife edge diffraction at the four edges of the rectangular screen, λ is the wavelength of the operating frequency, D_{2h_1} is the diffraction path length in edge h_1 and similar, r is the distance between Tx and Rx. Here, the basic diffraction gains of a rectangular screen (equivalent to the human body) F_{screen} were defined by the Fresnel-Kirchoff diffraction fundamentals [19, 27]. Analogous attenuation (L) is expressed as given in (29).

$$L = 1 - F_{\text{screen}} \quad (29)$$

Now, attenuation in decibels due to the human body (height h and width w) in terms of link blocking at the Rx is given in (30) through 3GPP model B.

$$L_{\text{dB}} = -20 \log_{10}(1 - (F_{h_1} + F_{h_2})(F_{w_1} + F_{w_2})) \quad (30)$$

2) 3GPP blockage model A

Our study focused on the Model A approach, where the blocker is modeled by a blocking region, in terms of center angle, elevation, and azimuth angular span around the user end under stochastic modeling. With model A, only the clusters are taken into consideration compared to model B, where the blocking fundamental is applied to the sub-path or ray and takes the lengths of the sub-paths that are blocked. Model A adheres to the steps outlined below.

Determine the number of blockers: The UE creates many 2-dimensional (2D) angular blocking zones around it. These regions are defined by their center angle, azimuth, and elevation angular span. There is a single zone that blocks itself named self-blocking region, and there are four regions that do not block themselves named non-self-blocking regions; the number of non-blocking regions may vary depending on specific conditions, such as a higher density of blockers. It is crucial to include the self-blocking component of the model to accurately represent the impact of human body blocking.

Generate the size and location of each blocker: the self-blocking region is defined by elevation and azimuth angles (θ_C, ϕ_C) and angular span in elevation and azimuth (y_k, x_k). In the blocking region, attenuation is high, centered around mid-angle ϕ_C and θ_C in azimuth and elevation, respectively. This means the cluster is blocked if its arrival angle in azimuth and elevation are within the blockage region of the respective angular region that $\theta_{\text{ZoA}} \in \{\theta_C - x_k, \theta_C + x_k\}$ and $\phi_{\text{AoA}} \in \{\phi_C - y_k, \phi_C + y_k\}$. For non-self-blocking, $k=1, 2, \dots$ can be considered as per the availability of blockers in the present scenario. The angular variables in these blockage cases are given in Table VII, and the variable values are given in Table VIII.

TABLE VII: ANGULAR PARAMETERS OF BLOCKING REGION

Dimension	Center angle	Angular spread	Blockage region	
			Self-Blocking	Non-Self-Blocking
Azimuth	ϕ_C	x_k	$\phi_C \pm x_k / 2$	$\phi_C \pm x_k$
Elevation	θ_C	y_k	$\theta_C \pm y_k / 2$	$\theta_C \pm y_k$

TABLE VIII: BLOCKING PARAMETERS OF BLOCKAGE MODEL A

Scenario	ϕ_C	x_k	θ_C	y_k	r
Indoor	0° to 360°	15° to 45°	90°	15° to 45°	2 m
Outdoor	0° to 360°	5° to 15°	90°	5°	10 m

Determine the attenuation of each cluster due to blockers: For the self-blockage case, the attenuation of each cluster in the self-blocking region is 30 dB, whereas for non-self-blockage, this attenuation is given by (31)

$$L_{dB} = 20 \log_{10} \{1 - [F(a_1) + F(a_2)][F(z_1) + F(z_2)]\} \quad (31)$$

where

$$a_1 = \phi_{AOA} - (\phi_C + x_k), \quad a_2 = \phi_{AOA} - (\phi_C - x_k)$$

$$z_1 = \theta_{ZOA} - (\theta_C + y_k), \quad z_2 = \theta_{ZOA} - (\theta_C - y_k).$$

and the term $F(x)$ is given as

$$F(x) = s(x) \frac{1}{\pi} \operatorname{atan} \left(\frac{\pi}{2} \sqrt{\frac{1}{\lambda_0} r \left(\frac{1}{\cos(x)} - 1 \right)} \right) \quad (32)$$

where $s(x) = \begin{cases} +1 & \text{if } x \leq 0 \\ -1 & \text{if } x > 0 \end{cases}$, $x \in \{a_1, z_1\}$, term λ refers to the wavelength of the operating frequency, while r represents the distance between the blocker and the user equipment. The model's parameters logically show that when the blocker is close to the Rx, the blocking region is large, and vice versa. And then, one can deduce that the probability of cluster blockage is higher in the indoor environment than in the outdoor.

Spatial and temporal consistency of each blocker: A random variable with a uniform distribution determines the blocker's central position. These random variables are spatially consistent, and the two-dimensional auto-correlation function denoted as $R(\Delta_x, \Delta_t)$, maybe accurately characterized by an exponential function as given in (33).

$$R(\Delta_x, \Delta_t) = \exp \left(- \left(\frac{|\Delta_x|}{d_{\text{corr}}} + \frac{|\Delta_t|}{t_{\text{corr}}} \right) \right) \quad (33)$$

where d_{corr} is the spatial correlation distance for the random variable determining the center of the blocker for various scenarios, and correlation time $t_{\text{corr}} = d_{\text{corr}}/v$ with v is the speed of the moving blocker.

The rectangular blocker explanation is chosen for the self-blocking region with the explicit choices of (ϕ_C, θ_C) assumed here.

3) 5G NR communication link

The 5G New Radio communication link serves as the fundamental pathway for data transmission between the user equipment and the network in a 5G system. Its purpose is multifaceted, aiming to deliver a significantly enhanced mobile broadband experience, ultra-reliable low-latency communication, and massive machine-type communication that enables a wide range of new applications and services. These purposes of 5G NR are enabled by key features like mm-wave frequencies, massive MIMO, NR waveform, and network slicing.

The 5G NR communication process involves several stages in transmitter and receiver chains. The proposed paper considers the 5G downlink transmission chain for end-to-end data processing and evaluates the performance of the 5G NR link using a cluster channel model. In 3GPP, the transmission chain mainly consists of several blocks with their specific functions during communication as shown in Fig. 5. It illustrates that in the production of a transport block, it calculates and appends a series of cyclic redundancy check (CRC) bits, which then undergo low-density parity check (LDPC) channel encoding and rate matching processing. In the communication chain, the rate matching block (a part of DL-SCH) is used to adjust the number of bits on the LDPC encoder output based on the anticipated number of bits for a certain modulation and coding scheme (MCS) [16]. In this scenario, MIMO precoding adjusts the number of spatial layers (streams) to match the number of active antennas for transmission and uses CP-orthogonal frequency-division multiplex (OFDM) numerology before data transmission. We configure the chain for the CDL channel model between the Tx and Rx for further analysis.

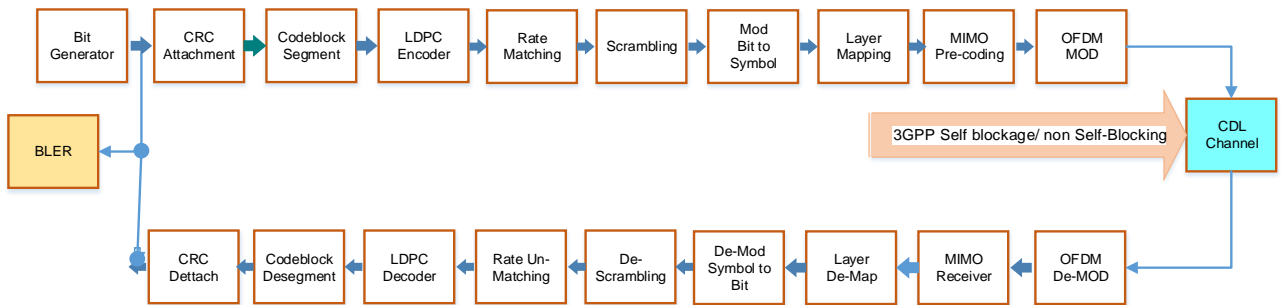


Fig. 5. 5G NR communication chain.

The receiver chain includes an equalization operation, whose objective is to counterbalance any distortions or fading that may have occurred to the signal during transmission across the channel. This communication chain applies the minimal mean square error (MMSE)

equalizer. A very important part of the process is soft demodulation, which changes the equalized data symbols into a set of values that LDPC decoding algorithms (a part of PDSCH) can easily understand. The descrambling process provides a known sequence of bits to allow for

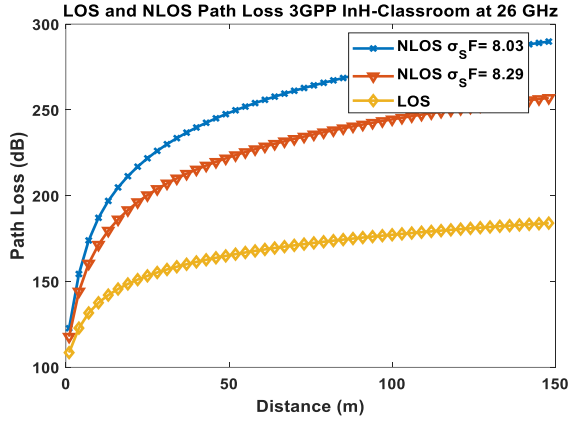


Fig. 8. Path loss (LOS and NLOS) in 3GPP InH at 5G FR1 and FR2.

We also assess the path loss estimate in the NLOS path at different shadow fading factors, demonstrating that path loss is more prominent in the NLOS path than in the LOS, as illustrated in Fig. 8. The higher value of shadow fading hurts the path loss estimate. These results are in agreement with the empirical results of other channel models [28] in a similar frequency range.

The CDL model is intended to establish a communication link with the cluster multipath, where the main parameters are cluster gain attenuation, delay spread, and angular spread. We simulate this communication link using a single BS and single user setup, ensuring that the blockage completely intersects the LOS path with the blocker's center, as shown in Fig. 3. The blockage scenario of the classroom is equivalently drawn in Fig. 3, depicting the angular blockage region of human blocking under 3GPP Blockage Model A.

Table X displays the blockage parameter in detail, taking into account the CDL-E profile and using the same antenna for both transmission and reception. In the 3GPP blockage model simulation for attenuation by the human body at 26 GHz, the center of the blocker is considered at azimuth $\phi_c = -180^\circ$ and elevation $\theta_c = 80.4^\circ$. This phenomenon of human blockage modeling is justified by a rectangular screen, whose diffraction losses are determined as per (31).

TABLE X: BLOCKAGE SIMULATION PARAMETERS

Simulation parameters	Parameter value
Channel model	3GPP LOS, CDL-E, $DS_{\text{desired}}=100\text{ns}$
Antenna model	3GPP Sector Antenna, Gain=8dBi(G_{max})
Carrier frequency	39 GHz, 26GHz
Bandwidth	400 MHz
Sub carrier spacing	120 kHz
Number of human blockers	One, two, three
Blockage region	$\phi_c = -180^\circ, x_k = 30^\circ, \theta_c = 80.4^\circ, y_k = 15^\circ, r=2\text{ m}$
Decoding algorithm	LDPC decoding, Normalized Min-Sum, Normalization factor $\alpha=0.7$
No of decoding iterations	50
Modulation, coding scheme	9
Size of FFT	4096

Here, we observe that the maximum signal power attenuation occurs when the blocker is at the center of the

screen, specifically at the LOS line, and it decreases as it approaches the screen's corner. For single blockers, we found the maximum attenuation to be 12.3 dB at the LOS line (center), and Fig. 9 demonstrates that attenuation decreases on both sides in azimuth spans up to 45° and in elevation spans up to 15° .

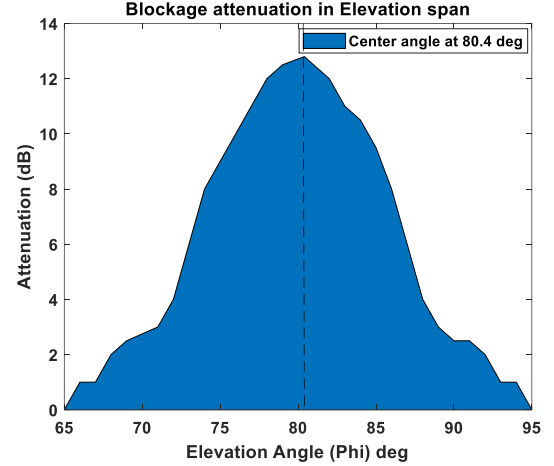


Fig. 9. Attenuation by human blockage in elevation span.

Similarly in azimuth span for single blockers, we found the maximum attenuation to be 12.3 dB at the LOS line (center), and the max attenuation decreases on both sides in azimuth spans up to 45° , whereas at 39 GHz this max attenuation reaches to 18.7 dB (at center) with a decreasing trend as shown in Fig. 10 towards both sides for azimuth span of 45° .

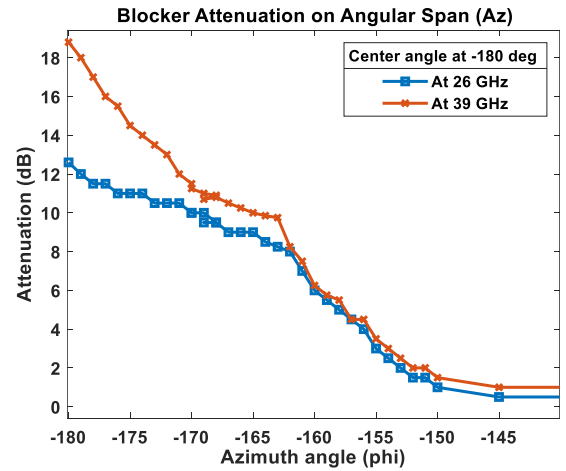


Fig. 10. Attenuation by human blockage in azimuth span.

Now, we looked at the CDL channel model with blockage conditions under multiple blocker conditions using the communication link shown in Fig. 5. As Fig. 11 illustrates, an increase in the number of blockers in the LOS path necessitates a higher SNR value to maintain the same BLER. This link-level simulation uses an MCS code rate of 0.6 at 16-QAM with an antenna gain of 8 dBi. As per [15], mm-wave provides an advantage on the eMBB use case of 5G, for which the target BLER is 10%. Based on Fig. 11, we can see that the SNR value for the target BLER changes, going from 13 dB when there is only one human blockage to 22.7 dB when there are two

human blockages and 29.5 dB when there are three human blockages compared to when there are no human blockages. This value matches the number that was calculated. The empirical model [45] also validated these results with comparable findings from the literature.

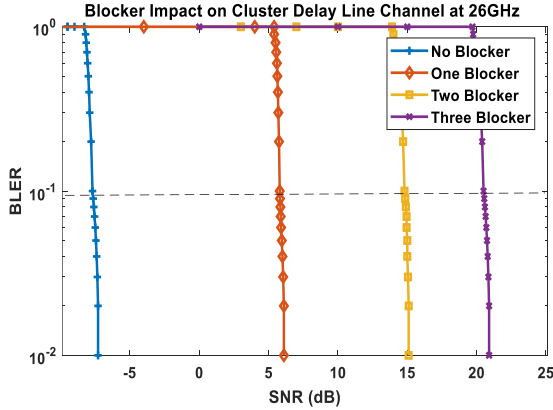


Fig. 11. SNR vs BLER of CDL model in blockage.

Another field of analysis uses link budget analysis for evaluation of the system capacity in terms of cell coverage in 5G communication, based on human attenuation and the number of human blockers, using Fig. 11. Table XI shows the basic parameters for link budget at the 26 GHz, where max path loss determines the cell range in various scenarios of human blockage. According to (3) and Fig. 11, a maximum path loss of 103.95 dB (no blocker) gives a cell range of 316 m, whereas a path loss of 95.55 dB (one blocker presence) reduces the cell range to 103 m. Further analysis reveals that two blockers (path loss of 86.45 dB) and three blockers (80.7 dB) correspond to max cell ranges of up to 26.95 m and 12.9 m, respectively. Prior research [15] confirmed the findings about diminished cell coverage for single blocker performance, and this study identified a similar pattern in multi-blockage scenarios. These results indicate that, when a blocker is present, it is necessary to progressively decrease the communication range to sustain equivalent service quality in the mm-wave band.

TABLE XI: LINK BUDGET PARAMETERS

Parameters	No blocker	One blocker	Two blockers	Three blockers
Tx power	10 dBm	10 dBm	10 dBm	10 dBm
Tx antenna gain	8 dBi	8 dBi	8 dBi	8 dBi
Rx antenna gain	8 dBi	8 dBi	8 dBi	8 dBi
EIRP	15 dBm	15 dBm	15 dBm	15 dBm
Rx noise figure	9 dB	9 dB	9 dB	9 dB
Rx sensitivity	-91.90 dBm	-78.50 dBm	-69.4 dB	-63.65 dB
Shadow margin	2.95 dB	2.95 dB	2.95 dB	2.95 dB
Max path loss	103.95 dB	95.55 dB	86.4 dB	80.7 db
Tx cable loss	3 dB	3 dB	3 dB	3 dB
Required SNR for 10% BLER	-7 dB	5.7 dB	14.8 dB	22.55 dB

Further analysis estimated the small-scale parameter (delay spread) for a specific case of indoor application as given in Table XII and carried out throughput simulations from the various CDL profile as shown in Fig. 12. Result on Fig. 12 shows that for the indoor scenario, with sub

carrier spacing 120 KHz and modulation (QAM=64), throughput of CDL-E performs better than CDL-A or CDL-B profile short and long delay spreads of 16 ns.

TABLE XII: PARAMETERS FOR INDOOR SCENARIO LINK LEVEL SIMULATION

S/N	Channel model	Environment	Proposed DS (ns)
1	CDL-A	NLOS	16
2	CDL-B	NLOS	16
3	CDL-C	NLOS	16
4	CDL-D	LOS	16
5	CDL-E	LOS	16

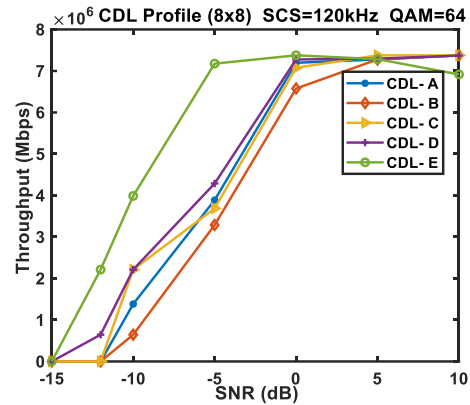


Fig. 12. Throughput of all CDL profiles in indoor scenario at DS of 16 ns, reduced DS considered due to human blockage.

The CDL link level simulation also uses the indoor scenario to simulate delay spread (DS), another cluster parameter that determines the response from the downlink 5G MIMO system. Human blockers can impact delay spread either by adding additional paths (increase DS) or by blocking existing paths (reduce delay spread). We assume in our study that blockage events do not alter the environment's state (LOS or NLOS) and that human blockers, by preventing the addition of new paths and clusters, only partially impact the cluster. Consequently, the blocker reduces delay spread by eliminating a specific number of multipath components. Here, the system under consideration is a downlink single-user multiple-input, multiple-output (MIMO) system.

Downlink single user MIMO consists of one BS with eight transmitter antennas and one User Equipment (UE) with eight reception antennas. The receiver utilizes minimum mean square error (MMSE) estimation. We select a carrier frequency of 26 GHz with a bandwidth of 100 MHz. The number of physical resource blocks (PRBs) allocated is quite suitable for configuration, and the duplex mode chosen is time division duplex (TDD). 64 QAM modulation is the modulation scheme used. Moreover, the simulations incorporate a delay scaling factor into the CDL channel models.

Therefore, we normalize the RMS delay spread values according to (9) and adjust them based on delay, which we can obtain from the reference [5]:

$$\tau_{n,\text{scaled}} = \tau_{n,\text{model}} \times \text{DS}_{\text{desired}} \quad (34)$$

where $\tau_{n,\text{scaled}}$ is the new delay value for n th cluster of CDL model, $\text{DS}_{\text{desired}}$ is desired DS and $\tau_{n,\text{model}}$ is the

normalized delay value for the n th cluster as per the 3GPP CDL delay profile. After the blockage event, we consider different DS, Table XII listed the values.

C. Evaluation of Outdoor Sports Ground Model

5G communication in outdoor and indoor scenarios differs significantly due to each environment's unique characteristics and challenges. The key difference lies in coverage, propagation, mobility, and use cases. Customization of our study on outdoor according to the 3GPP standard, treating this sports ground as an UMa 3GPP scenario. Physical parameters of the sports ground are given in Table XIII.

TABLE XIII: PHYSICAL PARAMETERS OF OUTDOOR SPORTS GROUND MODEL

Parameter subject	Parameter value	Remarks
Sports ground size	Radius 25m	Open roof
Capacity (person)	2500	Approximate
BS height (h_{BS})	25 m	Open place
Inter sight distance (ISD)	500 m	BS to UE
BS-UE min distance	35 m	-
UE height (h_{UE})	1.4 m	-
UE mobility	3 m/s	Static
Blocker type	Human	-
Blocker height (h_{BL})	1.7 m	-
Blocker state	Static/dynamic	Self/non-self
Standard	3GPP UMa	-

CDL channel parameters in the outdoor scenario vary from the indoor scenario for exact analysis; however, some parameters, such as the number of clusters, frequency of application, and polarization, remain similar to the indoor model. Sports grounds of radius R contain an open roof with BS antennas placed around the ground at height h_{BS} and distributed within the ground as per the poisson point process (PPP) model.

The density of BS in the ground is λ_T , the capacity for user equipment (UE) is about 2500, and there are evenly spaced static and dynamic blockers of height h_{BL} and densities of λ_B and λ_D . Here, we also assume that humans dominate the blocking region, ignoring the contribution of other available infrastructure at the sports ground during the study. People on the ground act as blockers in both self-blockage and non-self-blockage scenarios, exhibiting both static and dynamic blocker densities.

As shown in Fig. 13, the UMa sports ground scenario defines a large-scale parameter (path loss) in the LOS environment. The 3GPP standard estimates a large-scale parameter (path loss) in the LOS environment at various 5G operating frequency ranges of FR1 and FR2, and plots it in Fig. 14 [19], revealing a higher path loss at higher frequencies in the outdoor sports ground scenario. The path loss value keeps increasing as the separation distance between Tx and Rx increases. These results are in agreement with the empirical results of other channel models [33] in a similar frequency range.

Further, we estimated the small-scale parameter (delay spread) for a specific case of outdoor and carried out throughput simulations from the CDL-C and CDL-E profiles for the UMa scenario as shown in Table XIV.

With short and long delay spreads ranging from 75 ns to 720 ns, the links for the CDL-C profile (for the same communication link as in the indoor case) are simulated and plotted in Fig. 15. The findings indicate that outdoor performers perform better at higher delay spread values. On a similar kind of simulation, we used simulation for CDL-E at DS values of 75 ns and 400 ns and found that CDL-E slightly performs better in lower DS values.

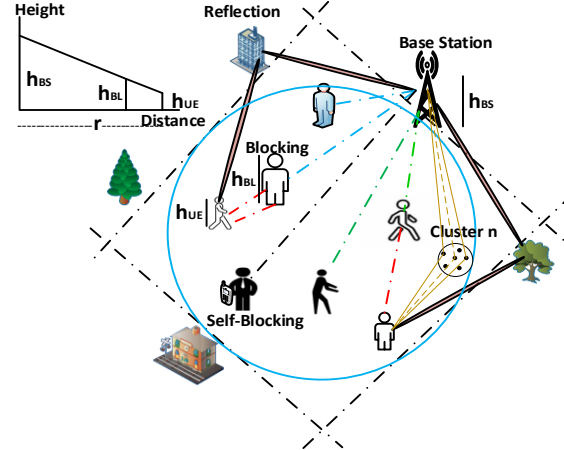


Fig. 13. Outdoor CDL model.

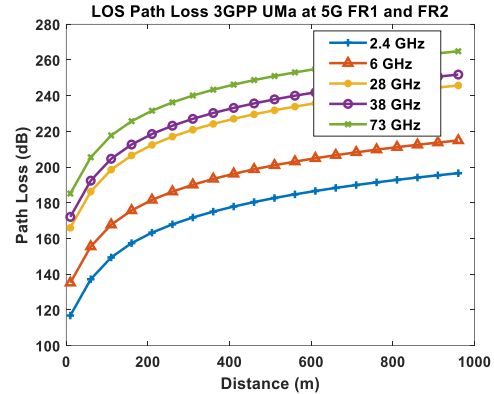


Fig. 14. UMa path loss at 5G frequencies.

TABLE XIV: PARAMETERS FOR OUTDOOR SCENARIO LINK LEVEL SIMULATION

S/N	Channel model	Environment	Proposed DS (ns)
1	CDL-C	NLOS	75
2	CDL-C	NLOS	720
3	CDL-E	LOS	72
4	CDL-E	LOS	400

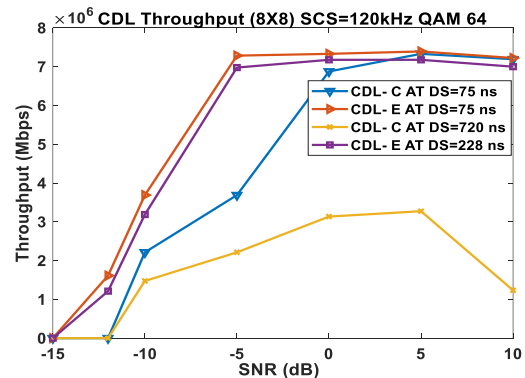


Fig. 15. Throughput of CDL profile in outdoor scenario at different delay spread.

The findings indicate that outdoors perform better at higher delay spread values. On a similar kind of simulation, we used simulation for CDL-E at DS values 75 ns and 400 ns and found that CDL-E slightly performs better in lower DS values. This indicates that the careful design of the 5G communication channel model is required in each scenario for URLLC and eMBB use case of 5G.

In LOS and NLOS cases, we also examine another quality performance parameter, coverage probability, about degrading performance due to static and self-blockage. In the presence of blockers (density λ_B) in the outdoor scenario, full radius coverage is provided in a certain probability if even a single BS is available for maintaining the link. LOS coverage probability is given by (35).

$$P(\text{cov}^{\text{LOS}}) = 1 - e^{-bc\lambda_T\pi R^2} \quad (35)$$

where $b=1 - \frac{\omega}{2\pi}$ is the probability of the link not being blocked, ω is self-blockage angle, c is the probability of the link being blocked as given in [12], λ_T is BS density. Further NLOS coverage probability is defined as per (36).

$$P(\text{cov}^{\text{NLOS}}) = 1 - e^{-c'\lambda_T\pi R^2} \quad (36)$$

where c' denotes the probability of link blocking, and all symbols are defined as per [12] for accurate analysis. While considering both LOS and NLOS links as potential links, the coverage is defined as the availability of at least one link and we assume the NLOS signal is large enough when BS is within the radius R . It is true that both the NLOS and LOS cases are well defined in the radius parameter and are independent of each other.

Coverage probability on given BS density under various self-blockage angles (ω) is shown in Fig. 16 indicating an increase in blocker density will reduce the probability of blockage. Similarly, an increase in BS density will improve the coverage, and self-blockage at zero degrees will have better coverage than any other blockage angle.

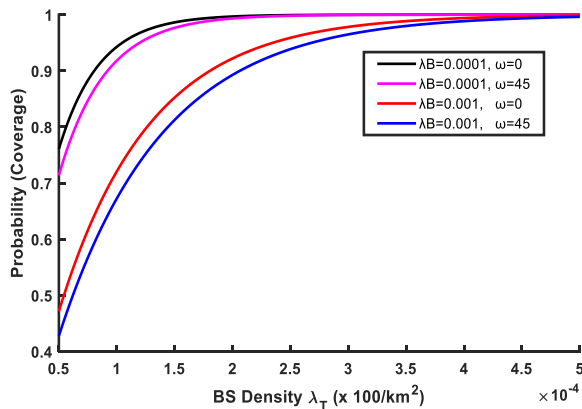


Fig. 16. Coverage probability on base station density for outdoor scenario.

V. CONCLUSION

The work proposes a CDL-based wireless channel model for 5G NR, in which cluster characteristics have

been considered as parameters to build the channel model statistically for indoor and outdoor scenarios. The 3GPP standard is used to model human blockage in the CDL channel. The impact of multiple human blockers, each with its own blockage angle, on 5G NR performance is examined. We analyze the PDSCH link level performance for QoS parameters such as throughput, BLER, and signal attenuation at 26 GHz and 39 GHz. The link budget estimation provides cell coverage analysis, and the results demonstrate how blockage and cluster parameters in the CDL channel play an important role in cell configuration when designing the mm-wave communication system for 5G applications. We analyze various parameters, such as delay spread, throughput, and outage probability, in both indoor and outdoor real-world scenarios. The future scope of this work lies in mitigating these human blockage impacts on 5G mm wave communication using various available techniques.

CONFLICT OF INTEREST

The authors declare no conflict of interest.

AUTHOR CONTRIBUTIONS

Conceptualization: Jai Kumar (J.K.) and Akhil Gupta (A.G.); writing- original draft preparation: J.K.; methodology: J.K. and A.G.; writing-review and editing: A.G.; software: J.K. and A.G.; visualization: J.K., Investigation: J.K and A.G. All authors have read and agreed to final version of manuscript.

ACKNOWLEDGEMENT

The authors gratefully acknowledge the Management, and Faculty of School of Electronics and Electrical Engineering, Lovely Professional University, Punjab, India for their support and for extending the necessary facilities to carry out this work.

REFERENCES

- [1] I. A. Hemadeh, K. Satyanarayana, M. El-Hajjar *et al.*, "Millimeter-wave communications: Physical channel models, design considerations, antenna constructions and link-budget," *IEEE Communications Surveys Tutorials*, vol. 20, no 2, pp. 870–913, Dec. 2017.
- [2] U. Karabulut, A. Awada, I. Viering *et al.*, "Low complexity channel model for mobility investigations in 5G networks," presented at 2020 IEEE Wireless Communications and Networking Conference, Seoul, Korea, 2020.
- [3] S. Sun, T. S. Rappaport, M. Shafi *et al.*, "Propagation models and performance evaluation for 5G millimeter-wave bands," *IEEE Trans. on Vehicular Technology*, vol. 67, pp. 8422–8439, Jun. 2018.
- [4] P. Ferrand, M. Amara, S. Vatinin *et al.*, "Trends and challenges in wireless channel modeling for evolving radio access," *IEEE Communications Magazine*, vol. 54, pp. 93–99, Jul. 2016.
- [5] G. Barb and M. Otesteanu, "On the influence of delay spread in TDL and CDL channel mm-wave models for downlink 5G MIMO systems," in *Proc. 2019 IEEE 10th Annual Ubiquitous Computing, Electronics Mobile Communication Conference*, New York, NY, USA, Oct. 2019, pp. 0958–0962.
- [6] A. Yaman and P. Spasojevic, "An intra-cluster model with diffuse scattering for communications: RT-ICM," *ArXiv*, ArXiv:1905.08295, May. 2019.
- [7] A. A. M. Saleh, and R. Valenzuela, "A statistical model for indoor

- multipath propagation," *IEEE Journal on Selected Areas in Communications*, vol. 5, no. 2, pp. 128–137, Feb. 1987.
- [8] J. Kumar and A. Gupta, "A review on 5G and beyond wireless communication channel models: Applications and challenges," *Physical Communication*, vol. 67, #102488, Dec. 2024.
- [9] S. Hur, S. Baek, T. S. Rappaport *et al.*, "Proposal on millimeter-wave channel modeling for 5G cellular system," *IEEE Journal of Selected Topics in Signal Processing*, vol. 10, no. 3, pp. 454–469, Apr. 2016.
- [10] G. R. MacCartney, T. S. Rappaport and S. Rangan, "Rapid fading due to human blockage in pedestrian crowds at 5G millimeter-wave frequencies," presented at 2017 IEEE Global Communications Conf., Singapore, 2017. doi: 10.1109/GLOCOM.2017.8254900
- [11] A. Alyosef, S. Rizou, ZD Zaharis *et al.*, "A survey on the effects of human blockage on the performance of mm wave communication systems," in *Proc. of 2022 IEEE Int. Black Sea Conf. on Communications and Networking*, Sofia, Bulgaria, Aug. 2022. doi: 10.1109/BlackSeaCom54372.2022.9858201
- [12] I. K. Jain, R. Kumar, and S. S. Panwar, "The impact of mobile blockers on millimeter wave cellular systems," *IEEE Journal on Selected Areas in Communications*, vol. 37, no. 4, pp. 854–868, 2018.
- [13] M. Gapeyenko, A. Samuylov, and M. Gerasimenko, "Analysis of human-body blockage in urban millimeter-wave cellular communications," in *Proc. of 2016 IEEE Int. Conf. on Communications*, Kuala Lumpur, Malaysia, 2016. doi: 10.1109/ICC.2016.7511572
- [14] S. Momo and M. Mowla, "Effect of human blockage on an outdoor mmWave channel for 5G communication networks," in *Proc. of 2019 22nd Int. Conf. on Computer and Information Technology*, Dhaka, Bangladesh, Dec. 2019. doi: 10.1109/ICCIT48885.2019.9038547
- [15] H. Dembele, M. L. Bot, F. Gallee *et al.*, "Impact of human blockage on 5G communication system in the 26 GHz band," in *Proc. of 2021 15th European Conf. on Antennas and Propagation (EuCAP)*, Dusseldorf, Germany, Apr. 2021. doi: 10.23919/EuCAP51087.2021.9411015
- [16] C. J. Pawase and KyungHi Chang, "5G-NR physical layer-based solutions to support high mobility in 6G non-terrestrial networks," *Drones*, vol. 7, no. 3, #176, 2023.
- [17] M. Dieng, G. Zaharia and G.E. Zein, "Wideband measurement and analysis of human blocking on the indoor radio channel at 60 GHz," in *Proc. of 2024 IEEE Wireless Communications and Networking Conf.*, Dubai, Apr. 2024. doi: 10.1109/WCNC57260.2024.10570684
- [18] M. Gapeyenko, A. Samuylov, D. Moltchanov *et al.*, "Spatially-consistent human body blockage modeling: A state generation procedure," *IEEE Trans. on Mobile Computing*, vol. 19, no. 9, pp. 2221–2233, Sep. 2020.
- [19] ITU, 3GPP, Study on channel model for frequencies from 0.5 to 100 GHz, European Telecommunications Standards Institute (ETSI), France, TR 38.901, v17.0.0 R17, Dec 2022.
- [20] D. Moltchanov and A. Ometov, "Analytical TCP model for millimeter-wave 5G NR systems in dynamic human body blockage environment," *Sensors*, vol. 20, no. 14, #3880, Jul. 2020.
- [21] C. Michael, "Physical-statistical channel model for signal effect by moving human bodies," *EURASIP Journal on Wireless Communications and Networking*, vol. 77, Mar. 2012. doi: 10.1186/1687-1499-2012-77
- [22] S. Parthasarathy, S. Kumar, R. K. Ganti *et al.*, "Error vector magnitude analysis in generalized fading with co-channel interference," *IEEE Trans. on Communication*, vol. 66, no. 1, pp. 345–354, Jan. 2018.
- [23] Y. Zhong, M. Haenggi, F. C. Zheng *et al.*, "Toward a tractable delay analysis in ultra-dense networks," *IEEE Communications Magazine*, vol. 55, no.12, pp. 103–109, Dec. 2017.
- [24] S. Sun, G. R. MacCartney and T. S. Rappaport *et al.*, "Millimeter-wave distance-dependent large-scale propagation measurements and path loss models for outdoor and indoor 5G systems," in *Proc. of 2016 10th European Conf. on Antennas and Propagation (EuCAP)*, Davos, Switzerland, Apr. 2016. doi: 10.1109/EuCAP.2016.7481506
- [25] S. Sun, T. S. Rappaport, A. Thomas *et al.*, "Investigation of prediction accuracy, sensitivity, and parameter stability of large-scale propagation path loss models for 5G wireless communications," *IEEE Trans. on Vehicular Technology*, vol. 65, no. 5, pp. 2843–2860, May 2016.
- [26] K. Haneda, L. Tian, H. Asplund *et al.*, "Indoor 5G 3GPP-like channel models for office and shopping mall environments," in *Proc. of 2016 IEEE Int. Conf. on Communications Workshops (ICC)*, Kuala Lumpur, Malaysia, May 2016. doi: 10.1109/ICCW.2016.7503868
- [27] K. Bhardwaj, A. Singh, and V. K. Sachan, "5G: An overview of channels characteristics and modeling techniques," in *Proc. of 2018 Fifth Int. Conf. on Parallel, Distributed and Grid Computing*, Solan, India, Dec. 2018. doi: 10.1109/PDGC.2018.8745875
- [28] G. MacCartney, T. S. Rappaport, S. Sun *et al.*, "Indoor office wideband millimeter-wave propagation measurements and channel models at 28 and 73 GHz for ultra-dense 5G wireless networks," *IEEE Access*, vol. 3, pp. 2388–2424, Oct. 2015.
- [29] S. Deng, M. Samimi and T. S. Rappaport, "28 GHz and 73 GHz millimeter-wave indoor propagation measurements and path loss models," in *Proc. of 2015 IEEE Int. Conf. on Communication Workshop*, London, Jun. 2015. doi: 10.1109/ICCW.2015.7247348
- [30] P. Kyosti, J. Meinila, Lassi Henttila *et al.* (2007). Technical report on project based WINNER II channel models. [Online]. Available: <https://www.cept.org/files/8339/winner2%20-%20final%20report.pdf>.
- [31] (Jul. 2015). Mobile and wireless communications enablers for the twenty-twenty information society (METIS). [Online]. Available: <https://cordis.europa.eu/project/id/671680>
- [32] C.-X. Wang, J. Bian, W. Zhang *et al.*, "A survey of 5G channel measurements and models," *IEEE Communications Surveys Tutorials*, vol. 20, no. 4, pp. 3142–3168, Aug. 2018.
- [33] K. Haneda, J. Zhang, L. Tan *et al.*, "5G 3GPP-like channel models for outdoor urban microcellular and macrocellular environments," in *Proc. of 2016 IEEE 83rd Vehicular Technology Conference (VTC Spring)*, Nanjing, China, Jul. 2016. doi: 10.1109/VTCSpring.2016.7503971
- [34] A. M. Pessoa, B. Sokal, C. F. Silva *et al.*, "A CDL-based channel model with dual-polarized antennas for 5G MIMO systems in rural remote areas," *IEEE Access*, vol. 8, pp. 163366–79, Sep. 2020.
- [35] J. Zhang, Z. Zhang, X. Wang *et al.*, "A simulated method of modeling wireless channel based on CDL," in *Proc. of 2010 Int. Conf. on Wireless Communications Signal Processing*, Suzhou, China, Oct. 2010. doi: 10.1109/WCSP.2010.5633447
- [36] X. Yin, C. Ling and M. D. Kim, "Experimental multipath-cluster characteristics of 28-GHz propagation channel," *IEEE Access*, vol. 3, pp. 3138–3150, 2015.
- [37] B. H. Fleury, M. Tschudin, R. Heddergott *et al.*, "Channel parameter estimation in mobile radio environments using the SAGE algorithm," *IEEE Journal on Selected Area in Communications*, vol. 17, no. 3, pp. 434–450, Mar.1999.
- [38] M.-Y. Gong and B. Lyu, "EM and SAGE algorithms for DOA estimation in the presence of unknown uniform noise," *Sensors*, vol. 23, no. 10, #4811, Mar. 2023. doi:10.3390/s23104811
- [39] Z. Fu, H. Cui, X. Zhao *et al.*, "An improved CDL model for 5G millimeter wave communication in a substation scenario," in *Proc. of 2020 IEEE Int. Conf. on Communications in China*, Chongqing, Aug. 2020. doi: 10.1109/ICCCWorkshops49972.2020.9209948
- [40] D. Cheng, J. Huang, S. Zhang *et al.*, "A novel approximate spectral clustering algorithm with dense cores and density peaks," *IEEE Trans. on Systems, Man, and Cybernetics Systems*, vol. 52, no. 4, pp. 2348–2360, Apr. 2022.
- [41] N. Kumari, S. Sharma and R. Rajput, "CDL channel model: revolutionizing wireless communication," *International Journal of Innovative Science and Research Technology*, vol. 8, no. 7, pp. 1937–1949, Jul. 2023.
- [42] M. Jiang, M. Hosseinian, M. Lee *et al.*, "3D channel model extensions and characteristics study for future wireless systems," in *Proc. of 2013 IEEE 24th Annual International Symposium on Personal, Indoor, and Mobile Radio Communications*, London, Sep. 2013. doi: 10.1109/PIMRC.2013.6666101
- [43] U. T. Virk and K. Haneda, "Modeling human blockage at 5G millimeter-wave frequencies," *IEEE Trans. on Antennas and Propagation*, vol. 68, no. 3, pp. 2256–2266, Mar 2020.
- [44] T. Jamsa, J. Medbo, P. Kyösti *et al.* "The 5G wireless propagation channel models," in *5G Mobile and Wireless Communications Technology*, A. Osseiran J. F. Monserrat P. Marsch, *et al.*, Ed., Cambridge: Cambridge University Press, June 2016.

[45] X. Zhao, Q. Wang, S. Li *et al.*, "Attenuation by human bodies at 26- and 39.5-GHz millimeter-wave bands," *IEEE Antennas and Wireless Propagation Letter*, vol. 16, pp. 1229–1232, Nov. 2016.

Copyright © 2025 by the authors. This is an open access article distributed under the Creative Commons Attribution License (CC BY 4.0), which permits use, distribution and reproduction in any medium, provided that the article is properly cited, the use is non-commercial and no modifications or adaptations are made.



Jai Kumar received the B.E. degree in electronics and communications engineering from Institution of Engineers India, Kolkata, India, in 2009, M.Tech. degree in electronics and communication from Punjab Technical University, Punjab, India, in 2013 and currently pursuing the Ph.D. degree in electronics and communication engineering at Lovely Professional University, Jalandhar, India. He is currently working in aviation

industry under Ministry of Defense, Government of India. He is a Member of Institution of Engineers India (MIE) and his research interest includes the emerging technologies, 5G wireless communication networks and currently doing his research work on channel modeling in 5G mm wave communication networks. He has published one book chapter and two research papers in International Journal.



Akhil Gupta (S'15-M'17-SM'22) received the B.E. degree in electronics and communication engineering from Jammu University, Jammu and Kashmir, India, in 2010, M.Tech. degree in electronics and communication engineering from the Jaypee University of Information Technology, Wanknaghat, India, in 2013 and Ph.D. degree in electronics and communication engineering from Shri Mata Vaishno Devi University, Jammu and Kashmir, India, in

2017. He is currently an associate professor in the School of Electronics and Electrical Engineering, Lovely Professional University, Punjab, India. He has guided 3 Ph.D. students and many master and undergraduate students. He has published >50 research papers, including IEEE Transactions, IEEE Journal, and also International Conference papers. His research interests include Physical and Network layer prospective of 5G and 6 G communications technologies such as NOMA, Cooperative wireless communications, Device to Device communications, Unmanned Ariel Vehicle, Massive MIMO, Cognitive Radio, Ultra Reliable Low Latency communication etc. He is also working on the security issues of next generation networks. He has been listed in the Top 2% scientist of the world by the Stanford University in four consecutive years (2020, 2021, 2022, 2013). He is also an author of the most popular paper in IEEE Xplore and an active reviewer of many IEEE, Springer, Elsevier, and Wiley Journals. He has also served as Keynote Speaker, session chair and technical program committee member for various international conferences. Dr. Gupta received the Teaching Assistantship at the Ministry of Human Resource Development from 2011 to 2013. He is a member of the International Association of Engineers and the Universal Association of Computer and Electronics Engineers, and has >3596 Citations in his credit.